Exploration of Rhenium Bisquinoline Tricarbonyl Complexes for their Antibacterial Properties

*Sofia Fulgencio[1], Mirco Scaccaglia[1,2], Angelo Frei[1,3]**

[1] Department of Chemistry, Biochemistry & Pharmaceutical Sciences, University of Bern, Freiestrasse 3, 3012 Bern, Switzerland
[2] Department of Chemistry, Life Sciences and Environmental Sustainability, University of Parma, 43124 Parma, Italy
[3] Department of Chemistry, University of York, York YO10 5DD, U.K.

E-mail: angelo.frei@unibe.ch

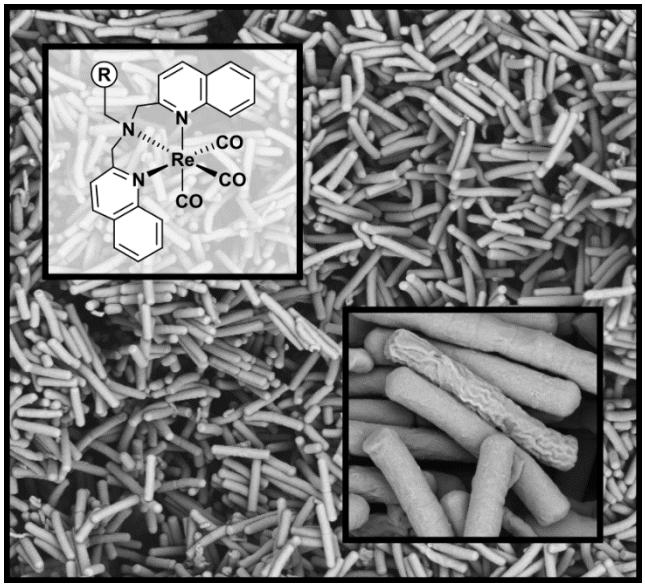

Abstract

Metal complexes have emerged as a promising source for novel classes of antibacterial agents to combat the rise of antimicrobial resistance around the world. In the exploration of the transition metal chemical space for novel metalloantibiotics, the rhenium tricarbonyl moiety has been identified as a promising scaffold. Here we have prepared eight novel rhenium bisquinoline tricarbonyl complexes and explored their antibacterial properties. Significant activity against both Gram-positive and Gram-negative bacteria was observed. However, all complexes also showed significant toxicity against human cells, putting into question the prospects of this compound class as metalloantibiotics. To better understand their biological effects, we conduct the first mode of action studies on rhenium bisquinoline complexes and show that they are able to form pores through bacterial membranes. Their straight-forward synthesis and tuneability suggests that further optimisation of this compound class could lead to compounds with enhanced bacterial specificity.

Introduction

Antibiotics are widely recognized pharmaceuticals with a global impact on public health and the treatment of infectious diseases which have significantly enhanced the overall quality of life. A crucial moment in their history was Paul Ehrlich's ground-breaking discovery of Salvarsan in 1909.[1] Following, investigations, compound 606, later named Salvarsan, exhibited promising efficacy in combating the Gram-negative bacterium *Treponema pallidum*,

responsible for syphilis.[2] In 1928, Alexander Fleming's discovery of Penicillin laid the foundation for the development of the first widely employed antibiotic.[3] This milestone not only holds immense significance in medical history but also catalyzed the era of antibiotics, revolutionizing the treatment of innumerable bacterial infections globally. The onset of antibiotics in clinical practice is widely regarded as one of the most monumental medical breakthroughs of the 20th century.[4] Nevertheless, the improper use of these compounds has led to an increase in antimicrobial resistance (AMR), giving rise to infections that are now nearly impossible to treat.[5] Predictions by the WHO predict that 5.2 million are expected to die from AMR in the Western Pacific Region alone by 2030.[6] This rise of multidrug-resistant (MDR) bacteria underscores the urgency for innovative medical solutions.[7]

In the realm of combating bacterial infections and the challenge of MDR bacteria, the pharmaceutical industry and medicinal chemistry predominantly favor organic compounds. This preference arises both from the immense success that organic molecules have had in medicinal chemistry as well as the perception that metals and their complexes primarily serve in material applications or catalytic functions, often associated with potential toxicity. However, despite this inclination, metal or inorganic complexes have historically demonstrated substantial contributions to medicine. Arsenic (Salvarsan) for the first syphilis treatment, mercury in antiseptic formulations like mercurochrome, and gold (Auranofin) for managing rheumatoid arthritis are prominent examples showcasing their medical applications.[8]

Auranofin is an FDA-approved organogold compound primarily designed for treating rheumatoid arthritis, has drawn attention due to its potential across various medical domains, including cancer[9], AIDS[10], parasitic[11] and bacterial infections.[12] Studies confirm the activity of auranofin against *M. tuberculosis, S. aureus, and Bacillus subtilis* strains *in vitro* and *in vivo*. Despite this, its activity against Gram-negative pathogens appears limited.[12] However, the FDA-approved status and established safety profile of auranofin in patients underline its potential as a prospective antibacterial medication. The approval of the platinum-based drug Cisplatin in 1978 solidified the significance of metal complexes in medicinal chemistry, continuing as a crucial component in most cancer treatments today.[13] Cisplatin, alongside carboplatin and oxaliplatin remains pivotal in numerous cancer treatments, such as testicular, ovarian, and lung cancer.[14]

In the last two decades more metal complexes have entered human clinical trials. These trials aim to explore their potential in treating cancer, malaria, and neurodegenerative diseases.[15] However, antibacterial applications within metal-based compounds have only received limited focus. Considering the extensive three-dimensional structural frameworks available through metal coordination chemistry they provide an ideal platform to explore novel antibiotic compounds, deviating from conventional two-dimensional structures. In recent research by Morrison *et al.*, an analysis revealed that a small library of 71 metal compounds encompassed a notably wider segment of the existing three-dimensional fragment space compared to the 18,534 organic fragments present in the ZINC database.[16] This observation emphasizes the potential of metal complexes in accessing previously unexplored three-dimensional chemical spaces, which holds relevance in medical chemistry associated with heightened target selectivity and reduced off-target effects.[17,18] In a key study, the Community for Open Antimicrobial Drug Discovery (CO-ADD) conducted a crowd-sourced screening of compounds against critical ESKAPE (*Enterococcus faecium*, *Staphylococcus aureus*, *Klebsiella pneumoniae*, *Acinetobacter baumannii*, *Pseudomonas aeruginosa*, and *Enterobacter spp.*) pathogens and two fungal species.[19] This extensive screening involved nearly 300,000 compounds, of which approximately 1000 belonged to the category of metal complexes. Interestingly, metal complexes exhibited an approximately tenfold higher hit rate (27%) against the ESKAPE pathogens in comparison to entirely organic compounds (1.6%). Contrary to the

assumption that metal compounds inherently pose more toxicity, the assessed metal compounds demonstrated comparable cytotoxicity to human embryonic kidney (HEK293) cells and a similar haemolytic effect on human red blood cells (hRBC) in relation to the tested organic compounds.[20,21]

Within this diverse landscape of metal compounds, rhenium, often overshadowed by other metals like iron and ruthenium in medicinal applications, has garnered increasing attention. Ongoing research has unveiled the diverse potential of rhenium(I) complexes in medicinal chemistry, particularly their applications as anticancer agents, imaging agents for radiopharmaceuticals, and more recently, as antibacterial agents.[22–26]

The investigation conducted by the Bandow and Metzler-Nolte research groups stands as an early milestone in the elucidation of the antibacterial potential of rhenium(I) tricarbonyl complexes and comprehending their mechanism of action. Their study included the synthesis of **1** (Figure 1), a trimetallic complex comprising rhenium, iron, and manganese integrated within a peptide nucleic acid framework. Notably, **1** demonstrated antibacterial activity against diverse Gram-positive bacteria, including methicillin resistant *S. aureus* (MRSA), vancomycin-intermediate *S. aureus* (VISA), and *B. subtilis*. No activity against Gram-negative bacteria was observed. Delving deeper into the mode of action, the researchers examined the relationship between the structure and antibacterial activity of the compound. Their investigations highlighted the pivotal role of the Re-containing **[(dpa)Re(CO)$_3$]** moiety and their antibacterial activity. Further systematic modification of **1** by substituting the metal-containing portions with simpler organic functions revealed the crucial role of the rhenium tricarbonyl component for its antibacterial activity. While alterations in the **ferrocene** and **manganese** fragments did not significantly alter the antibacterial activity, the presence of rhenium component proved indispensable for maintaining the antibacterial properties. In more in-depth studies **1** and its ruthenium analogue were observed to disturbed crucial processes at the bacterial cell membrane and impeding respiration and cell wall biosynthesis. Of note compound **1** displayed limited solubility in water and bacterial growth media (≤ 25 µg/mL). The cytotoxicity of **1** was tested in a range of human cell lines (healthy and cancerous) and signs of toxicity where observed in MCF7 (human epithelial breast cancer cell line, IC_{50} < 3 µg/mL), NRK-52E (rat kidney epithelial cell line, 55% viability at 25 µg/mL) and CCRF-CEM (human T-cell lymphoblast cell line, 57% viability at 25 µg/mL).[27,28]

The group of Zobi reported on a series of rhenium tricarbonyl complexes in recent years with some (e.g. **2**) showing activity against Gram-positive bacteria in zebrafish *in vivo* infection models. While the antibacterial activity of the best compounds was higher than their toxicity, some detrimental effects against zebrafish were observed at higher concentrations.[29,30]

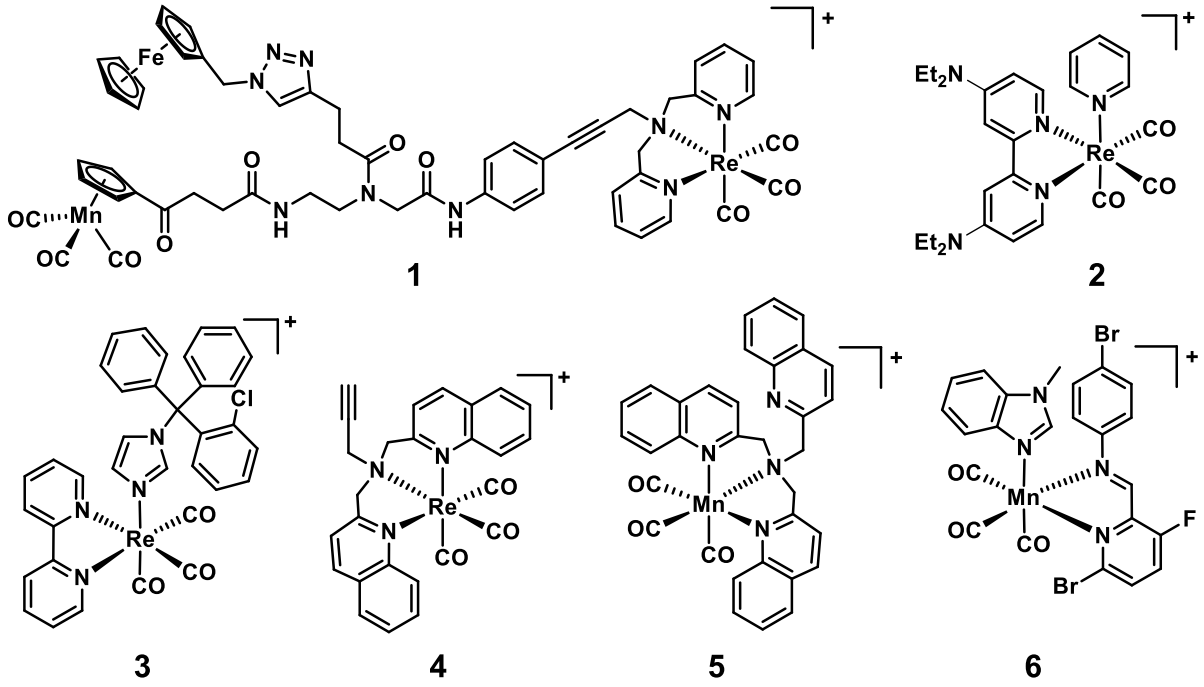

Figure 1. Selected chemical structures of $M(CO)_3$ (M = Re, Mn) compounds with reported antibacterial properties.

In more recent work Mendes et al. delved into another rhenium compound, **3**, subjected to an in-depth mechanism-of-action investigation. These investigations revealed its mode of action, targeting the cytoplasmic membrane to potentially disrupt peptidoglycan synthesis. This exploration was motivated by the substantial activity, blood stability, and the absence of carbon monoxide release. This compound exhibited remarkable minimal inhibitory concentration (MIC) of 0.5 µg/mL against MRSA and promising activity against various Gram-negative strains, including *Escherichia coli* (16 µg/mL) and *Acinetobacter baumannii* (8 µg/mL). However, **3** also showe high levels of cytotoxicity against HepG2 (human hepatic, IC_{50} = 1.4 ± 0.4 µM) and LLC-PKI cells (porcine kidney, IC_{50} = 2.0 ± 0.8 µM).[31]

In other work Frei *et al.*, extended the scope of rhenium(I) complexes with bisquinoline and tricarbonyl moieties (**4**). These compounds exhibited dual mode of action against both Gram-positive and Gram-negative bacteria, notably demonstrating enhanced activity upon light activation against Gram-positive strains while requiring light exposure for activity against Gram-negative bacteria. Lead compound **4** displayed moderate toxicity in the dark (CC_{50} = 59.9 ± 9.2 µM) against human embryonic kidney (HEK293) cells which was enhanced upon light irradiation (CC_{50} = 19.1 ± 5.7 µM).[32]

Overall, the promise of rhenium(I) tricarbonyl has been shown, however in many of the reports, hints of cytotoxicity, albeit at generally higher concentrations than their MIC, were described. It should be noted that manganese(I) tricarbonyl compounds, sharing the same group as rhenium(I) and being isoelectronic with it, have also been found to possess promising antibacterial properties by our group and others.[33–35]

Based on this previous work we aimed to expand our investigation of rhenium(I) bisquinoline (Bq) tricarbonyl complexes. Herein eight novel ReBq complexes were synthesized, fully characterized and assessed for their biological properties including *in vitro* antibacterial activity and toxicity studies as well as an exploration of the mechanism of action of this compound class.

Results and Discussion

Synthesis of Bisquinoline Ligands

The ligands synthesis was performed via a reductive amination by Sodium triacetoxyborohydride (STAB) involving two equivalents of 2-Quinolinecarboxaldehyde and one equivalent of different amines (Figure 2).[32] The reactions were monitored using a Liquid Chromatography Mass Spectrometry (LC-MS) system. The determination of the reaction completion was primarily based on the visual observation of the reaction mixture´s color, which appeared as a bright orange color in all ligands. Initially, ligands **L1-3** were purified through a process involving their dissolution in methanol, followed by stirring for 10 min to gently quench the STAB reagent. Afterwards, methanol was evaporated, re-introduced, and the mixture was subjected to filtration, with the filtrate retained. Subsequently, another round of methanol evaporation dissolution and evaporation was performed, and the resulting reaction mixture was dissolved in dichloromethane (DCM), followed by filtration to maintain the filtrate. However, in the later phases of the project, this purification step proved to be counterproductive, as it led to the formation of more side products prior to the workup, as observed through LC-MS analysis. Furthermore, it was determined that purifying the ligands was unnecessary, given the successful performance of complex synthesis even in the absence of ligand purification. The Ligands **L1-L9** were characterized by LC-MS and Nuclear Magnetic Resonance (NMR).

Synthesis of Small Complex Library

The complex synthesis was performed as previously reported by reacting [$ReCO_5Br$] with the ligands in methanol under microwave irradiation (Figure 2).[32] To confirm the presence of the desired compound, LC-MS analysis was conducted post-reaction, consistently revealing the desired masses. The subsequent purification of **Re1**-**Re3** was achieved through precipitation with ammonium hexafluorophosphate. On the other hand, the other rhenium complexes (**Re4** -**Re9**) underwent purification via preparative reverse-phase liquid chromatography (RP-HPLC). While RP-HPLC resulted in a lower overall yield, the outcome was notably improved in terms of purity. Following purification, the complexes were characterized by LC-MS, ^{1}H and ^{13}C NMR and High-Resolution MS.

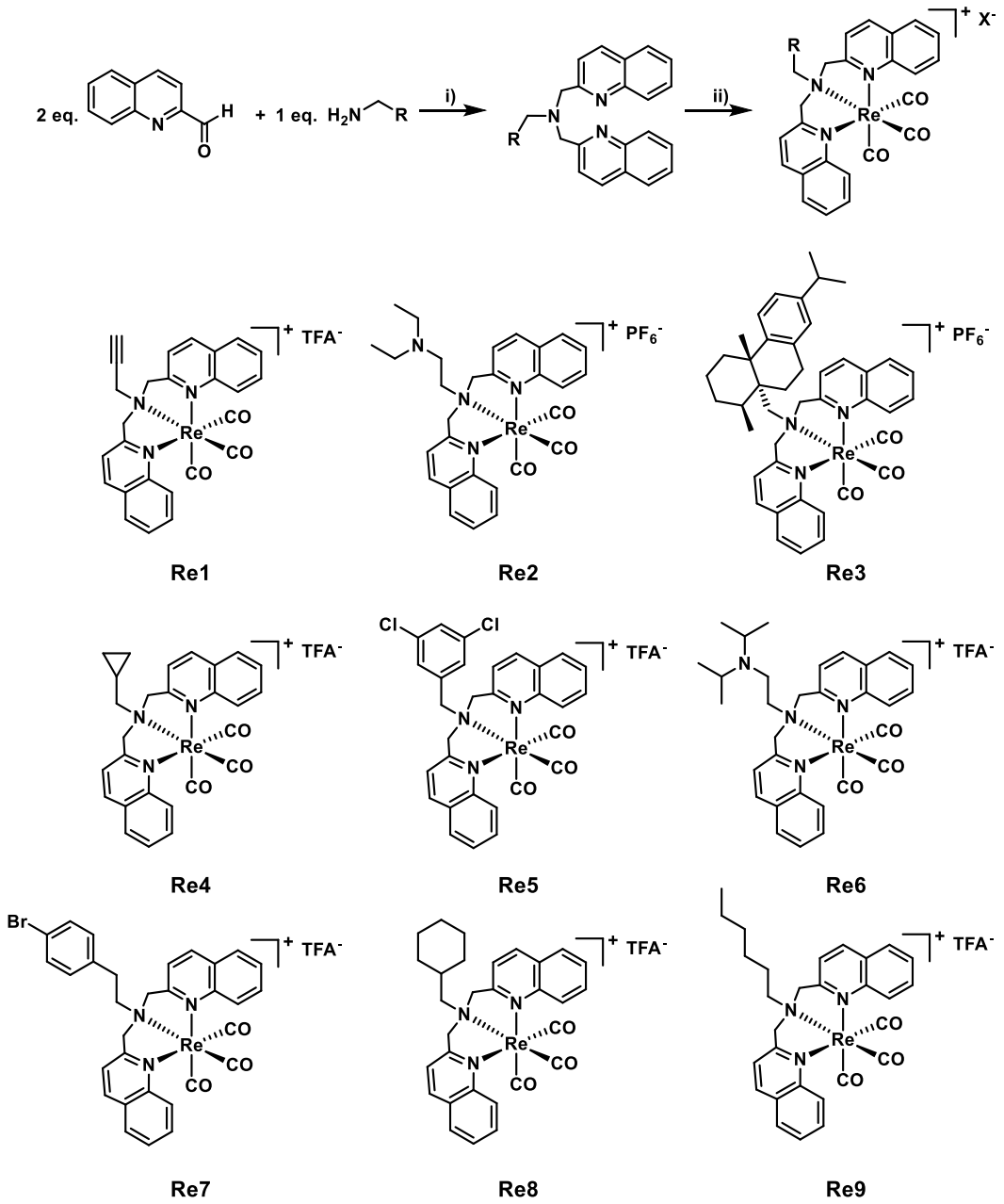

Figure 2. (Top) General reaction scheme for the preparation of rhenium bisquinoline tricarbonyl complexes. i) $Na[(CH_3COO)_3BH]$, DCE, 0 °C, 2 h; r.t., 16 h. ii) MeOH, MW 120 °C, 1 h. (Bottom) Structure of the nine novel rhenium complexes prepared in this work.

Rhenium Complex Stability.

To evaluate whether the studied rhenium bisquinoline complexes remain intact during their biological assessment we investigated the stability of all nine complexes by UV/Vis absorbance in different solvents (DMSO and HEPES buffer) at 37 °C, over time to monitor any changes (Figure S1). The majority of all complexes showed no significant changes in absorption over 18 h in any solvent. For **Re7** a small decrease in absorbance in the aqueous solvent was observed. Overall, all compounds remained largely unchanged in the temperature and time window relevant for the biological experiments.

Antibacterial Activity

Table 1. Antibacterial activity against a selection of Gram-positive and Gram-negative strains, toxicity data in HEK293T cells and human red blood cells for the 9 synthesized compounds.

	MIC [µM]					Toxicity [µM]	
	MRSA	**MSSA**	***B. subtilis***	***E. coli***	***A. baumannii***	**HC_{10}**	**CC_{50}**
Re1	3.13 - 6.25	3.13 - 6.25	6.25	50 - >100	100 - >100	>200	14 ± 4
Re2	12.5	12.5	12.5	>100	>100	93 ± 1	9 ± 2
Re3	12.5	6.25	6.25 - 12.5	50 - >100	>100	66 ±7	4 ± 1
Re4	1.56	1.56	3.125	25 - 100	25-50	157 ± 5	5 ± 2
Re5	≤0.78 - 1.56	≤0.78 - 1.56	≤0.78 - 1.56	12.5 - 25	12.5	38 ± 5	7 ± 1
Re6	1.56 - 6.25	3.13 - 6.25	3.13	25 - 100	25 - 50	>200	5 ± 1
Re7	0.78 - 1.56	≤0.78 - 1.56	1.56	12.5 - 25	12.5 - 25	29 ± 6	6 ± 1
Re8	≤0.78 - 1.56	≤0.78 - 1.56	≤0.78 - 1.56	12.5 - 25	12.5	45 ± 3	4 ± 1
Re9	≤0.78 - 1.56	≤0.78 - 1.56	≤0.78 - 1.56	12.5 - 25	12.5 - 25	31 ± 4	3 ± 1
Ctrl [µg/mL]	0.5	0.25 - 1	≤ 0.125	0.25 - 1	0.25 - 1		

Antibacterial activity is displayed as MIC [µM]. MRSA – methicillin resistant *S. aureus*; MSSA – methicillin susceptible *S. aureus*; HC_{10} – Human red blood cells; CC_{50} – HEK293T cells; Ctrl = Vancomycin for MRSA, MSSA, and *B.* subtilis. Ctrl = Polymyxin B for *E. coli* and *A. baumannii*; TI – therapeutic index, determined by dividing the lowest value between CC_{50} and HC_{50} with the lowest MIC value for each compound; MIC determined with n=4 across two biological replicates.

To determine the MIC of the synthesized rhenium(I)Bq complexes the broth microdilution method was performed. The antibacterial activity of the rhenium complexes was evaluated against a panel of Gram-positive (MRSA; MSSA – methicillin susceptible *S. aureus*; *B. subtilis*) and Gram-negative bacteria (*E. coli*; *A. baumannii*; PAO1 – *P. aeruginosa*). Additionally, since previous work suggest light irradiation could enhance the antibacterial properties of ReBq compounds[32], the rhenium complexes synthesized in this work were subjected to light irradiation (at 405 nm for 10 minutes using a Atlas Photonics LUMOS BIO irradiator) for *E. coli* and MRSA. However, no heightened antibacterial activity was observed following light irradiation. Consequently, light irradiation was excluded from subsequent assays. All MIC values are displayed in Table 1.

All tested compounds exhibited varying degrees of activity against Gram-positive and Gram-negative bacteria. The lowest activity was observed against the tested Gram-positive bacteria for **Re2** (12.5 µM), followed by **Re3** (ranging from 6.25 to 12.5 µM), **Re1** (6.25 µM), **Re4** (3.13 µM), and **Re6** (3.13 µM) (**Table 2**). In contrast, **Re5**, **Re8**, and **Re9** displayed identical MIC values (ranging from 1.56 to ≤0.78 µM), indicative of potent antibacterial activity against the tested Gram-positive bacteria. The tested rhenium(I) complexes displayed no to moderate activity against the tested Gram-negative bacteria. Moderate activity against *E. coli* and *A. baumannii* was observed with values of 12.5 – 50 µM. The rhenium(I) complexes **Re5, Re7, Re8** and **Re9** display the best activity among the tested compounds against the two previously mentioned Gram-negative bacteria. While **Re1** to **Re3** displayed no antibacterial activity against *A. baumannii*, **Re4** and **Re6** exhibited minimal antibacterial activity with relatively high MIC values (25-50 µM). The other rhenium compounds, particularly **Re5, Re7-Re9**, demonstrated the lowest MIC values, with **Re5** and **Re8** both showing an MIC of 12.5 µM. While these MIC values are not ideal, they do indicate some potential for the compounds.

In contrast, no antibacterial activity was observed against *P. aeruginosa* and *K. pneumoniae* for any of the compounds. In previous work, **Re1** was tested against multiple drug-resistant strains, including *K. pneumoniae, A. baumannii*, and *P. aeruginosa*.[32] No activity against *K. pneumoniae* and only moderate activity against *A. baumannii* and *P. aeruginosa* was noted when subjected to light irradiation at 365 nm. The MIC values for **Re1** in the literature were >186.2 µM for *K. pneumoniae* in the dark, 186.2 µM for *A. baumannii*, and 93.1 µM for PAO1. These values are generally consistent with the MICs measured by us, except for PAO1, where the measured MIC was consistently higher than 100 µM. This alignment between the obtained data and literature findings adds confidence to the reproducibility of the results.

In conclusion, all rhenium(I) complexes (**Re1-Re9**) exhibited antibacterial activity against Gram-positive bacteria. Among these, the most promising candidates are **Re5** and **Re7-Re9**. Firstly, they demonstrate superior activity against Gram-positive bacteria compared to the other compounds. Secondly, they also display moderate activity against Gram-negative bacteria, such as *E. coli* and *A. baumannii*.

Toxicity and Haemolysis

In order to determine potential toxicity of the synthesized complexes their haemolytic and cytotoxic properties were determined. Haemolysis was determined against human red blood cells (hRBC) using a previously reported protocol.[35] The data were fit to determine the HC_{10} i.e. the concentration of compound that causes 10% haemolysis. The cytotoxcitiy of the rhenium complexes was determined against human embryonic kidney HEK293T cells utilizing a standard MTT assay. The compounds displayed strongly variable levels of haemolysis (Table 1) with some showing no detectable effect up to 200 µM (**Re1** and **Re6**) and others showing strong haemolysis (**Re7** and **Re9**). Surprisingly all rhenium complexes showed significant cytotoxicity against the HEK293T cells. Apart from **Re1** which still displayed a CC_{50} of 14±4 µM all other compounds had single digit micromolar CC_{50} values. In order to explore possible correlations between the structure of the compounds and their cytotoxicity, we calculated the logP values of the nine bisquinoline ligands (as proxies for the rhenium complex logP) and compared the results with their corresponding HC_{10} and CC_{50} values (Figure S2). A weak but consistent trend can be observed, i.e. higher lipophilicity tends to correlate with a higher degree of haemolysis and toxicity (or lower HC_{10} and CC_{50} values). In previous work a CC_{50} value of 59.9 ± 9.2 µM was found for **Re1** against HEK293 cells[32] which is significantly higher than what was obtained here, highlighting the strong variability that is inherent to any biological experiment.

Bacterial cytological profiling of Re8

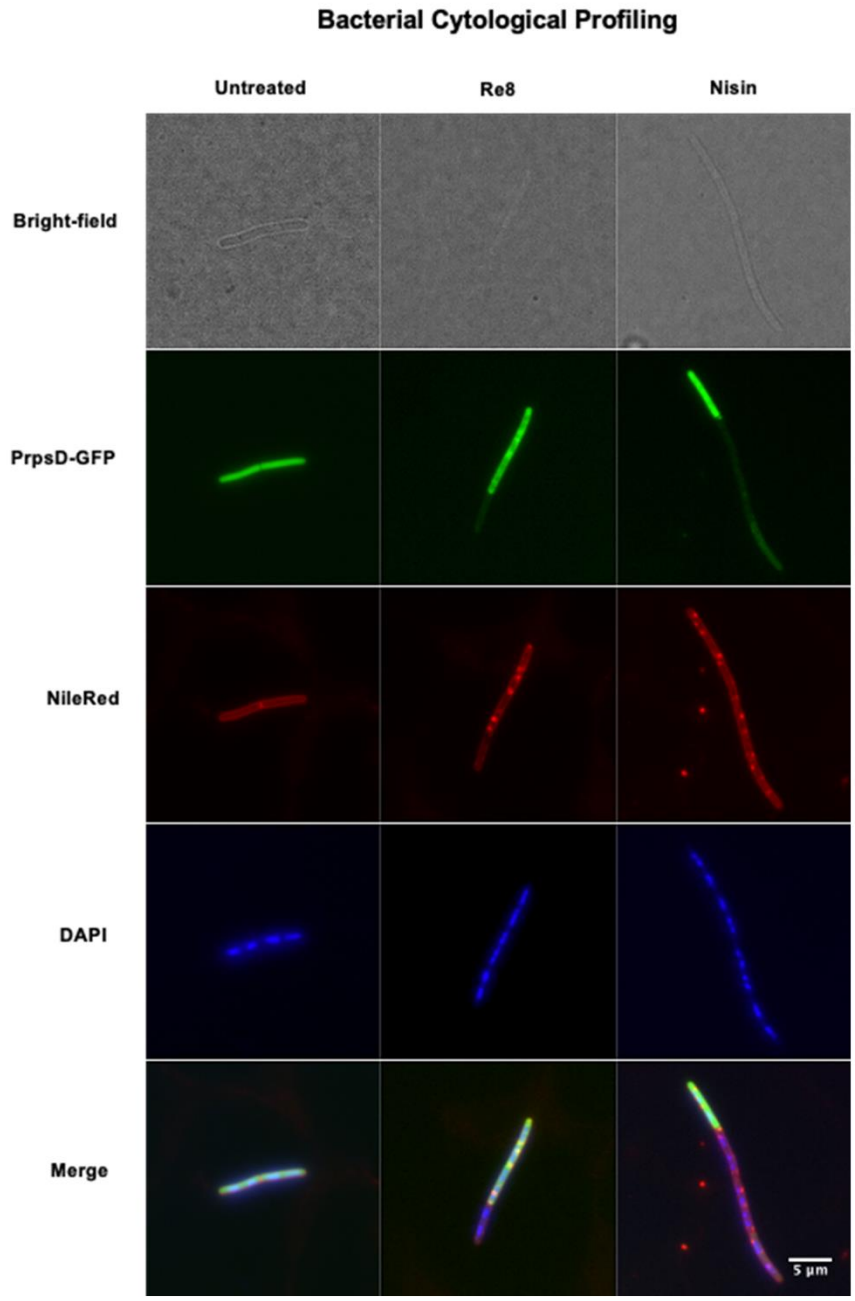

Figure 3. Fluorescence microscopy pictures obtained. BCP: *B. subtilis* bSS82 PrpsD strain incubated with 1.56 µM **Re8** for 10 min and stained with DAPI (1 µg/mL) and Nile red (0.5 µg/mL) compared with untreated control and Nisin (100 µg/mL).

We selected **Re8** for preliminary mode of action (MoA) studies to better understand the effect of the rhenium compounds on bacteria, as well as to start understanding the possible factors contributing to the general cytotoxicity. As **Re3-9** displayed virtually identical levels of cytotoxicity we chose **Re8** for further studies as it has the highest ratio between its HC_{10} value and MIC against MRSA (~29).

The mode of action of Re8 on bacteria was investigated through bacterial cytological profiling (BCP) experiments using the Gram-positive *Bacillus subtilis* model strain.[35,36] Briefly, *B. subtilis* bSS82[37], expressing cytosolic GFP from the robust ribosomal PrpsD promoter was

incubated with **Re8** for 10 min before the DNA stain DAPI and the membrane stain Nile red were added, and the bacteria were imaged with a fluorescence microscope. The **Re8**-treated bacteria images were compared with untreated and nisin-treated control groups (Figure 3). Nisin is an antibacterial peptide chosen as the positive control, inhibits cell-wall biosynthesis, forming large pores, disrupting membrane potential, and causing nutrient and ion leakage.[38–40] Compared to the untreated control, clear differences were visible in the GFP, Nile red and DAPI signal. The presence of bacterial cells with depleted GFP signal as well as strong spot-formation in the Nile red signal was observed which is very similar to the effect caused by the nisin control suggesting a similar mode of action.

Effect of Re8 on the bacterial membrane

As the BCP results suggested that **Re8** has an effect on the bacterial membrane, we conducted experiments to interrogate this further. Given MinD's role in cell division regulation, we incubated a MinD-GFP *B. subtilis* LH131 reporter with both **Re8** and the positive control compound, nisin. The resulting effects were visualized using fluorescence microscopy (Figure 4A). Under normal circumstances, MinD localizes around the bacterial cell poles and septa.[36,41] The fluorescence pictures show a strong delocalization of MinD under the influence of both nisin and **Re8**. This effect is different to the one observed in our previous work with a manganese tricarbonyl compound (compound **6**, Figure 1) where the membrane was similarly targeted, yet the compound demonstrated the ability to release COs, and consequently inhibiting the respiratory chain.[35] This adds further support to the hypothesis that **Re8** detrimentally affects the bacterial membrane. Additionally, the similarity of the effects observed between the pore-forming nisin and **Re8** point towards a similar MoA for the metal compound. Further evidence for this was provided by a propidium iodide (PI) influx assay. PI can only cross membranes if they have been strongly compromised e.g. by a pore-forming compound. Indeed, both **Re8** and nisin resulted in a strong increase in fluorescence in the bacteria which was not observed in the untreated sample (Figure 4B). A clear effect on the membrane potential by **Re8** was demonstrated by a $DiOC_2$ assay. A depolarization effect comparable to the one of the ionophore gramicidin was observed (Figure 4C). Altogether these assays suggest that the antibacterial effect of **Re8** is caused, by forming pores in the bacterial membrane which lead to bacterial death.

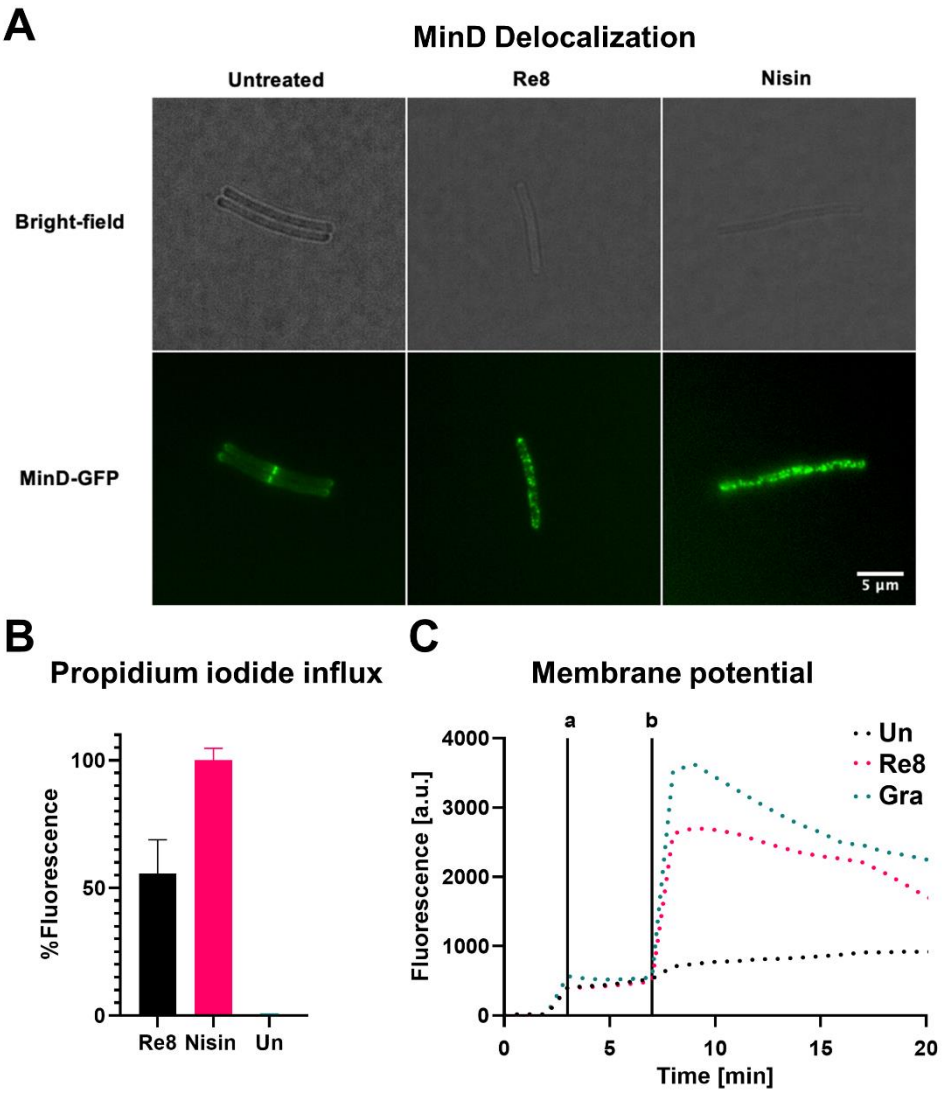

Figure 4. (**A**) *B. subtilis* LH131 with MinD reporter incubated with 1.54 µM **Re8** for 10 min compared with untreated control and Nisin (100 µg/mL). **(B)** Quantified PI fluorescence in bacteria after exposure to **Re8** (1.56 µM, 15 min), Nisin (positive control, 50 µg/mL, 15 min) or no compound. (**B**) $DiOC_2$ fluorescence as a measure of membrane depolarisation after addition of **Re8** (1.56 µM), gramicidin (positive control 1 µg/mL). a) indicates the time point of $DiOC_2$ addition b) indicates the time point of antibiotic addition.

SEM imaging of Re8

Having narrowed the primary effect of **Re8** to the damaging the bacterial membrane we aimed to further visualize this. Hence we exposed *B. subtilis* 168CA to different concentrations of **Re8** and prepared scanning electron microscopy (SEM) samples based on previous reports.[42,43] Untreated samples were used as negative controls and indeed intact bacteria could be visualized (Figure 5A-B). Bacterial samples exposed to sodium dodecyl sulfate (SDS), a pore-forming surfactant, showed clearly visible effects on the outer membrane (Figure 5C-D), which looked deformed and ‘wrinkled‘. In some cases, distinct ‚holes‘ and ‚tears‘ could be observed which were not found in the untreated sample. Samples treated with **Re8** showed similarly pronounced effects on the membrane. At around the MIC concentration of 1.56 µM not all cells were equally affected but effects similar to the SDS samples could be observed (Figure 5E-F). At elevated concentrations of **Re8** (1 mM) most bacterial cells showed similar effects with numerous forms of membrane damage visible. Taken together with the

other experiments, these pictures provide substantial evidence that **Re8** acts by damaging the membrane of bacteria.

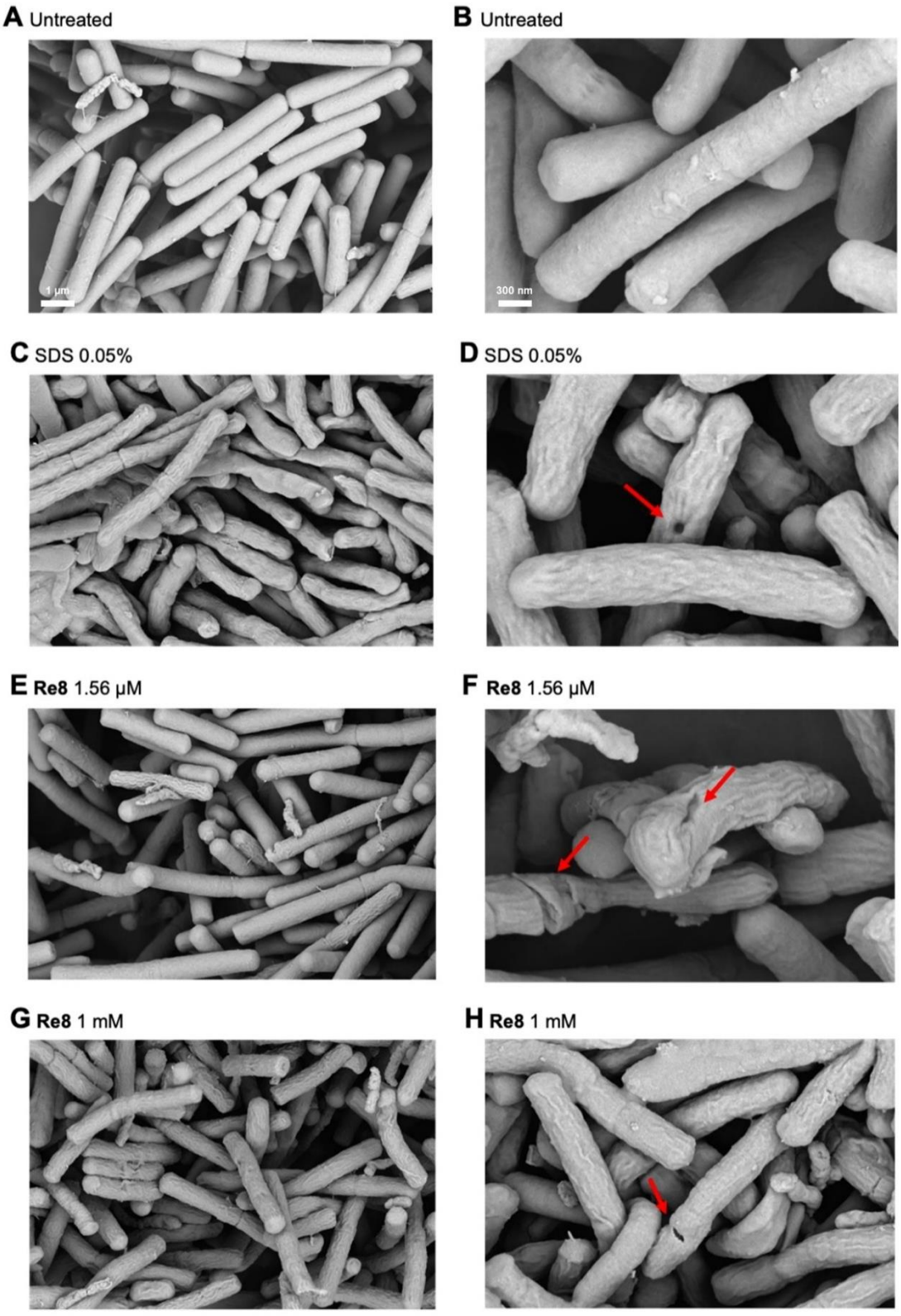

Figure 5. SEM images of *B. subtilis* 168CA (**A-B**) untreated control (**C-D**) SDS positive control (0.05%) (**E-F**) *B. subtilis* incubated with **Re8** (1.56 µM) for 10 min (**G-H**) *B. subtilis* 168CA incubated with **Re8** (1 mM) for 10 min.

Conclusion

We have further explored the family of rhenium bisquinoline tricarbonyl complexes by synthesizing, purifying and completely characterizing eight novel derivatives. We found that most of these complexes showed high antibacterial activity against Gram-positive strains with some even showing activity against two Gram-negative strains i.e. *E. coli* and *A. baumannii*. Surprisingly, unlike in earlier work, the antibacterial activity of most complexes could not be enhanced by light irradiation at 405 nm suggesting that specific structural features contribute to the light-enhanced activity. Additionally, all compounds showed significant cytotoxic effects against mammalian cells and some haemolysis, reducing their potential as antibacterial agents. To better understand their biological effects, we probed the mechanism of action of this compound class for the first time by conducting BCP microscopy studies with one representative compound. Initial experiments indicated a strong effect of the rhenium complex on bacterial membranes. Follow-up experiments that focused on membrane effects revealed that these compounds are likely to form pores, similar to the antibacterial peptide nisin and the ionophore gramicidin. Lastly, we were able to image the effect of one rhenium complex on the bacterial membrane by SEM imaging. It is possible that these compounds cause similar damage to mammalian cell membranes, potentially explaining their elevated cytotoxicity. Due to their otherwise strong antibacterial properties and ease of diversification we think it is worth exploring other compounds in this class with improved selectivity for bacterial membranes e.g. by introducing more positive charges and/or bacterial targeting vectors.

Experimental Section

Materials and Reagents.

All reagents were commercially available, and they were used without any further purification.

Physical Measurements

Analytical RP-HPLC−MS was performed with an Ultimate 3000 Rapid Separation LC−MS System (DAD-3000RS diode array detector) using an Acclaim RSLC 120 C18 column (2.2 µm, 120 Å, 3 × 50 mm, flow 1.2 mL/min) from Dionex. The HPLC is directly linked to a Thermo Scientific LCQ- Fleet Ion-trap MS. The elution solutions were A: MilliQ deionized water containing 0.05% TFA and D: MilliQ deionized water/acetonitrile (10:90,v/v) containing 0.05% TFA. High resolution mass spectra were recorded from LTQ Orbitrap XL with nano ESI (Thermo) positive mode, samples prepared in acetonitrile. NMR were recorded from AVANCE II 400 MHz (Bruker). UV-vis spectra were collected using 1 cm quartz cuvette at room temperature with a Shimadzu UV-1800 UV spectrophotometer. Microwave reactions were conducted with Biotage Initiator.

General Ligand Synthesis

2-Quinolinecaboxaldehyde (100 mg, 0.64 mmol) and the corresponding amine (0.32 mmol) were dissolved into 10 mL of 1,2-Dichlorethane (DCE). The reaction mixture was then stirred at room temperature under an argon atmosphere and protected from light for 2 hours. Subsequently, sodium triacetoxyborohydride (STAB) (1.11 mmol) was added to the reaction mixture at 0 °C, and the reaction was then stirred under an argon atmosphere, protected from light, overnight. The solvent was removed from the reaction mixture *in vacuo*. This resulted in the formation of a brightly coloured orange-white solid. No further purification was performed for **L3-6** & **L8-9**. Ligands **L1**,**L2** & **L7** were purified as follows: The crude was dissolved in

approximately 20 mL of methanol and stirred at room temperature for 10 minutes. The methanol was then evaporated, and 20 mL of methanol was added again. The mixture was filtered, keeping the filtrate. The solvent was evaporated, and 20 mL dichloromethane (DCM) was added. The mixture was cooled down to 0 °C and then filtered again keeping the filtrate. To obtain the pure solid, DCM was evaporated. For **L1**, an additional purification step was carried out by adding acetonitrile and filtering it again, keeping the filtrate.

L1. Corresponding amine: Propargylamine. Yield 20-60 %. MW 337.4 $gmol^{-1}$. ESI-MS (+, m/z, $[M+Na]^+$): 360.25 $[C_{23}H_{19}N_3Na]^+$. HR-MS (+, m/z, $[M+Na]^+$) $[C_{23}H_{19}N_3Na]^+$ calculated: 360.1471; found: 360.1458. ^1H NMR (300 MHz, $CDCl_3$) δ 8.10 (dd, J = 13.0, 8.6 Hz, 4H), 7.78 (d, J = 9.0 Hz, 2H), 7.73 – 7.65 (m, 4H), 7.54 – 7.47 (m, 2H), 4.14 (s, 4H), 3.51 (d, J = 2.3 Hz, 2H), 2.32 (t, J = 2.3 Hz, 1H).

L2. Corresponding amine: 2-Diethylaminoethylamine. Yield 83 %. MW 398.5 $gmol^{-1}$. HR-MS (+, m/z, $[M+H]^+$) $[C_{26}H_{31}N_4]^+$ calculated: 399.2543; found: 399.2529. ^1H NMR (300 MHz, $CDCl_3$) δ 8.13 (d, J = 8.4 Hz, 2H), 8.05 (d, J = 8.5 Hz, 2H), 7.78 (d, J = 8.1 Hz, 2H), 7.68 (ddd, J = 8.4, 6.9, 1.4 Hz, 2H), 7.61 (d, J = 8.5 Hz, 2H), 7.51 (ddd, J = 8.0, 7.1, 1.1 Hz, 2H), 4.07 (s, 4H), 3.13 (dd, J = 8.7, 5.1 Hz, 2H), 3.01 (dd, J = 8.8, 5.0 Hz, 2H), 2.86 (q, J = 7.3 Hz, 4H), 1.05 (t, J = 7.3 Hz, 6H).

L3. Corresponding amine: (+)-dehydroabietylamine. Yield 22 %. MW 567.8 $gmol^{-1}$. ESI-MS (+, m/z, $[M+H]^+$): 568.43 $[C_{40}H_{46}N_3]^+$. HR-MS (+, m/z, $[M+H]^+$) $[C_{40}H_{46}N_3]^+$ calculated: 568.3686; found: 568.3665. ^1H NMR (300 MHz, $CDCl_3$) δ 8.05 (t, J = 8.1 Hz, 4H), 7.77 (d, J = 9.0 Hz, 2H), 7.71 – 7.65 (m, 4H), 7.50 (t, J = 7.0 Hz, 2H), 7.15 (d, J = 8.2 Hz, 1H), 6.97 (d, J = 9.8 Hz, 1H), 6.79 (s, 1H), 4.08 (d, J = 10.3 Hz, 4H), 2.84 – 2.77 (m, 3H), 1.64 – 1.57 (m, 2H), 1.50 – 1.42 (m, 2H), 1.42 – 1.28 (m, 2H), 1.21 (d, J = 6.9 Hz, 6H), 1.15 (s, 3H), 0.97 – 0.81 (m, 4H), 0.80 (s, 3H), 0.71 (d, J = 1.4 Hz, 1H).

L4. Corresponding amine: Cyclopropabemethylamine. MW 353.5 $gmol^{-1}$. ESI-MS (+, m/z, $[M+Na]^+$): 353.19 $[C_{24}H_{23}N_3Na]^+$. HR-MS (+, m/z, $[M+H]^+$) $[C_{24}H_{24}N_3]^+$ calculated: 354.1965; found: 354.1953. ^1H NMR (300 MHz, $CDCl_3$) δ 8.09 (dd, J = 16.8, 8.5 Hz, 4H), 7.83 – 7.75 (m, 4H), 7.67 (t, J = 7.6 Hz, 2H), 7.49 (t, J = 7.4 Hz, 2H), 4.13 (s, 4H), 2.53 (d, J = 6.6 Hz, 2H), 0.99 (dt, J = 12.3, 5.4 Hz, 1H), 0.45 (d, J = 7.2 Hz, 2H), 0.09 (d, J = 4.5 Hz, 2H).

L5. Corresponding amine: 3,5-Dichlorobenzylamine. MW 458.4 $gmol^{-1}$. ESI-MS (+, m/z, $[M+H]^+$): 458.11 $[C_{27}H_{22}Cl_2N_3]^+$. ^1H NMR (300 MHz, $CDCl_3$) δ 8.16 (d, J = 8.5 Hz, 2H), 8.08 (d, J = 8.5 Hz, 2H), 7.79 (d, J = 8.1 Hz, 2H), 7.69 (dd, J = 13.4, 7.9 Hz, 4H), 7.51 (t, J = 7.5 Hz, 2H), 7.31 (s, 2H), 7.18 (s, 1H), 4.02 (s, 4H), 2.16 (s, 2H).

L6. Corresponding amine: N,N-Diisopropylethane-1,2-diamine. MW 426.6 $gmol^{-1}$. ESI-MS (+, m/z, $[M+Na]^+$): 449.42 $[C_{28}H_{34}N_5Na]^+$. ^1H NMR (300 MHz, $CDCl_3$) δ 8.15 (d, J = 8.5 Hz, 2H), 8.05 (d, J = 8.5 Hz, 2H), 7.79 (d, J = 8.1 Hz, 2H), 7.67 (dd, J = 18.7, 8.1 Hz, 4H), 7.51 (t, J = 7.4 Hz, 2H), 4.12 (s, 4H), 3.52 – 3.41 (m, 2H), 3.12 (s, 4H), 1.14 (s, 12H).

L7. Corresponding amine: 4-Bromophenethylamine. MW 482.4 $gmol^{-1}$. ESI-MS (+, m/z, $[M+H]^+$): 482.17 $[C_{28}H_{25}BrN_3]^+$. ^1H NMR (300 MHz, $CDCl_3$) δ 8.06 (d, J = 8.4 Hz, 4H), 7.79 (d, J = 8.0 Hz, 2H), 7.69 (t, J = 8.2 Hz, 2H), 7.52 (dd, J = 7.8, 3.9 Hz, 4H), 7.26 (s, 2H), 6.92 (d, J = 8.3 Hz, 2H), 4.07 (s, 4H), 2.92 – 2.79 (m, 4H).

L8. Corresponding amine: Cyclohexane methylamine. MW 395.5 $gmol^{-1}$. ESI-MS (+, m/z, $[M+H]^+$): 396.33 $[C_{27}H_{30}N_3]^+$. ^1H NMR (300 MHz, $CDCl_3$) δ 8.13 (d, J = 8.5 Hz, 2H), 8.06 (d, J = 8.4 Hz, 2H), 7.81 – 7.74 (m, 4H), 7.71 – 7.64 (m, 2H), 7.53 – 7.46 (m, 2H), 3.97 (s, 4H), 2.39 (d, J = 7.1 Hz, 2H), 2.08 (s, 1H), 1.87 (d, J = 13.0 Hz, 2H), 1.65 (d, J = 11.8 Hz, 2H), 1.17 (t, J = 11.1 Hz, 2H), 0.73 (q, J = 14.2, 13.4 Hz, 2H).

L9. Corresponding amine: Hexylamine. MW 383.5 $gmol^{-1}$. ESI-MS (+, m/z, $[M+H]^+$): 384.25 $[C_{26}H_{30}N_3]^+$. ^1H NMR (300 MHz, $CDCl_3$) δ 8.12 (d, J = 8.5 Hz, 2H), 8.06 (d, J = 8.5 Hz, 2H), 7.76 (t, J = 8.1 Hz, 4H), 7.71 – 7.64 (m, 2H), 7.53 – 7.46 (m, 2H), 4.01 (s, 4H), 2.65 – 2.56 (m, 2H), 1.57 (p, J = 7.2 Hz, 2H), 1.31 – 1.14 (m, 6H), 0.80 (t, J = 6.9 Hz, 3H).

General Rhenium Complex Synthesis

Pentacarbonylchlororhenium (30 mg, 0.083 mmol) and the corresponding ligand (0.083 mmol) were dissolved in 3 mL of methanol inside a Biotage microwave vial with a capacity of 2-5 mL. The reaction mixture was subjected to microwave heating at 120 °C for 1 hour using a Biotage Inititator. After the reaction, the solvent was evaporated, and a yellowish solid was obtained. Purification for **Re3-9** was achieved through preparative high-performance liquid chromatography using the following conditions: flow rate of 40 mL/min, solvent A: 0.1% trifluoroacetic acid (TFA) in water, and solvent D: 90% acetonitrile (ACN) and 10% water with 0.1% TFA. The program used: A/D 90:10 to 0:100 in 60 min. The resulting fractions were collected, and their purity was verified by LC-MS using the following conditions: flow rate of 1.2 mL/min, solvent A: 0.1% TFA in water, and solvent D: 90% ACN and 10% water with 0.1% TFA. The LC-MS program used: A/D 100:0 to 0:100 in 10.00 min or 5 min, total absorbance and then subjected to lyophilization.

Re1. Yield 29%. MW 704.68 $gmol^{-1}$. Analytical RP-HPLC: t_R = 4.8 min. ESI-MS (+, m/z, $[M]^+$): 608.12 $[C_{26}H_{19}N_3O_3Re]^+$. HR-MS (+, m/z, $[M]^+$): $[C_{26}H_{19}N_3O_3Re]^+$ calculated: 608.0978; found: 608.0973. ^1H NMR (400 MHz, CD_3CN) δ 8.52 (dd, J = 8.6, 3.1 Hz, 4H), 8.04 (dd, J = 8.2, 1.3 Hz, 2H), 7.91 (ddd, J = 8.7, 7.0, 1.5 Hz, 2H), 7.75 – 7.69 (m, 2H), 7.57 (d, J = 8.5 Hz, 2H), 5.17 (d, J = 17.8 Hz, 2H), 4.98 (d, J = 17.8 Hz, 2H), 4.63 (d, J = 2.5 Hz, 2H), 3.07 (t, J = 2.5 Hz, 1H). ^{13}C NMR (101 MHz, CD_3CN) δ 165.48, 147.89, 142.47, 134.08, 130.64, 129.54, 129.40, 129.25, 120.95, 80.13, 77.35, 69.73, 57.02.

Re2. Yield 51%. MW 813.76 $gmol^{-1}$. Analytical RP-HPLC: t_R = 3.7 min. ESI-MS (+, m/z, $[M]^+$): 669.36 $[C_{29}H_{30}N_4O_3Re]^+$. HR-MS (+, m/z, $[M]^+$): $[C_{29}H_{30}N_4O_3Re]^+$ calculated: 669.1870; found: 669.1848. (+, m/z, $[M+PF_6+H]^+$): $[C_{29}H_{31}F_6N_4O_3PRe]^+$ calculated: 815.1590; found: 815.1571. (+, m/z, $[M-PF6]^{2+}$): $[C_{29}H_{31}N_4O_3Re]^{2+}$ calculated: 335.0972; found: 335.0961. ^1H NMR (400 MHz, CD_3CN) δ 8.50 (dd, J = 14.3, 8.5 Hz, 4H), 8.03 (dd, J = 8.1, 1.3 Hz, 2H), 7.91 (ddd, J = 8.7, 7.0, 1.5 Hz, 2H), 7.75 – 7.70 (m, 2H), 7.54 (d, J = 8.5 Hz, 2H), 5.17 – 4.95 (m, 4H), 4.28 – 4.19 (m, 2H), 3.69 – 3.58 (m, 2H), 3.32 (s, 4H), 1.35 (t, J = 7.3 Hz, 6H). ^{13}C NMR (101 MHz, CD_3CN) δ 165.10, 147.86, 142.79, 134.24, 130.78, 129.64, 129.42, 129.31, 120.98, 69.14, 60.99, 49.58, 49.19, 9.12.

Re3. Yield 11%. MW 983.02 $gmol^{-1}$. Analytical RP-HPLC: t_R = 7.5 min ESIMS (+, m/z, $[M]^+$): 838.53 $[C_{43}H_{45}N_3O_3Re]^+$. HR-MS (+, m/z, $[M]^+$): $[C_{43}H_{45}N_3O_3Re]^+$ calculated: 838.3013; found: 838.2992. ^1H NMR (400 MHz, CD_3CN) δ δ 8.66 (d, J = 9.3 Hz, 1H), 8.46 (d, J = 8.4 Hz, 1H), 8.37 (d, J = 8.4 Hz, 1H), 8.15 (d, J = 8.9 Hz, 1H), 8.00 – 7.93 (m, 3H), 7.72 (td, J = 7.8, 7.4,

1.0 Hz, 1H), 7.69 – 7.62 (m, 2H), 7.59 (ddd, J = 8.0, 7.0, 1.1 Hz, 1H), 7.41 (d, J = 8.5 Hz, 1H), 7.22 (d, J = 8.2 Hz, 1H), 7.02 (dd, J = 8.2, 2.0 Hz, 1H), 6.93 (d, J = 2.0 Hz, 1H), 5.44 – 5.28 (m, 3H), 5.05 (d, J = 18.1 Hz, 1H), 4.29 (d, J = 14.5 Hz, 1H), 4.09 (d, J = 14.5 Hz, 1H), 2.96 (dd, J = 17.1, 6.7 Hz, 1H), 2.83 (ddt, J = 20.8, 13.8, 7.2 Hz, 2H), 2.39 (t, J = 11.4 Hz, 2H), 2.14 (s, 11H), 1.44 (s, 2H), 1.30 (s, 2H), 1.18 (d, J = 6.9 Hz, 6H). ^{13}C NMR (101 MHz, CD_3CN) δ 167.79, 165.96, 148.52, 147.72, 147.44, 146.98, 142.42, 142.12, 135.53, 134.11, 133.61, 130.57, 129.72, 129.41, 129.18, 129.14, 129.11, 128.79, 127.86, 124.97, 121.60, 120.83, 80.71, 70.37, 69.39, 48.41, 44.10, 40.70, 39.00, 38.62, 34.31, 30.88, 25.96, 24.31, 24.28, 20.62, 19.98, 19.43.

Re4. Yield 11-25%. MW 721.12 gmol^{-1}. Analytical RP-HPLC: t_R = 5.15 min. ESI-MS (+, m/z, $[M]^+$): 624.22 $[C_{27}H_{23}N_3O_3Re]^+$. HR-MS (+, m/z, [M]+): $[C_{27}H_{23}N_3O_3Re]$+ calculated: 624.1291; found: 624.1283. ^{1}H NMR (300 MHz, CD_3CN) δ 8.50 (dd, J = 12.8, 8.6 Hz, 4H), 8.01 (d, J = 8.2 Hz, 2H), 7.89 (ddd, J = 8.7, 7.0, 1.5 Hz, 2H), 7.70 (t, J = 7.6 Hz, 2H), 7.56 (d, J = 8.5 Hz, 2H), 5.20 (d, J = 17.8 Hz, 2H), 4.99 (d, J = 17.8 Hz, 2H), 3.70 (d, J = 6.8 Hz, 2H), 1.27 (s, 1H), 0.82 (d, J = 7.5 Hz, 2H), 0.57 (d, J = 5.2 Hz, 2H).^{13}C NMR (101 MHz, CD_3CN) δ 166.16, 147.90, 142.44, 134.01, 130.63, 129.48, 129.44, 129.19, 121.02, 72.51, 69.55, 8.91, 5.09.

Re5. Yield 21%. MW 825.64 gmol^{-1}. Analytical RP-HPLC: t_R = 5.87 min. ESI-MS (+, m/z, $[M]^+$): 728.18 $[C_{30}H_{21}Cl_2N_3O_3Re]^+$. HR-MS (+, m/z, [M]+): $[C_{30}H_{21}Cl_2N_3O_3Re]^+$ calculated: 728.0512; found: 728.0488. ^{1}H NMR (400 MHz, CD_3CN) δ 8.51 (d, J = 8.8 Hz, 2H), 8.46 (d, J = 8.4 Hz, 2H), 8.02 – 7.97 (m, 2H), 7.89 (s, 2H), 7.70 (d, J = 7.1 Hz, 5H), 7.51 (d, J = 8.4 Hz, 2H), 5.20 (d, J = 17.5 Hz, 2H), 5.03 (s, 2H), 4.67 (d, J = 17.6 Hz, 2H). ^{13}C NMR (101 MHz, CD_3CN) δ 165.52, 147.86, 142.50, 136.42, 136.24, 134.06, 132.04, 130.69, 130.63, 129.47, 129.37, 129.27, 121.19, 69.35, 68.41.

Re6. Yield 18%. MW 796.86 gmol^{-1}. Analytical RP-HPLC: t_R = 3.83 min. ESI-MS (+, m/z, $[M]^+$): 697.25 $[C_{31}H_{44}N_4O_3Re]^+$. HR-MS (+, m/z, $[M]^+$): $[C_{31}H_{44}N_4O_3Re]^+$ calculated: 697.2183; found: 697.2171. ^{1}H NMR (400 MHz, CD_3CN) δ 8.47 (d, J = 8.8 Hz, 4H), 8.00 (d, J = 7.9 Hz, 2H), 7.90 – 7.84 (m, 2H), 7.69 (t, J = 7.5 Hz, 2H), 7.53 (d, J = 8.3 Hz, 2H), 5.29 (d, J = 17.6 Hz, 2H), 5.15 (d, J = 17.7 Hz, 2H), 4.50 (s, 2H), 3.77 (s, 2H), 3.65 (s, 2H), 1.44 (d, J = 6.3 Hz, 12H). ^{13}C NMR (101 MHz, CD_3CN) δ 196.79, 194.78, 165.62, 147.76, 142.53, 134.02, 130.66, 129.47, 129.30, 129.26, 120.95, 69.02, 62.56, 55.77, 43.04, 18.47.

Re7. Yield 15%. MW 849.68 gmol^{-1}. Analytical RP-HPLC: t_R = 6.07 min. ESI-MS (+, m/z, $[M]^+$): 752.24 $[C_{31}H_{24}BrN_3O_3Re]^+$. HR-MS (+, m/z, $[M]^+$): $[C_{31}H_{24}BrN_3O_3Re]^+$ calculated: 752.0553; found: 752.0526. ^{1}H NMR (400 MHz, CD_3CN) δ 8.50 (d, J = 8.5 Hz, 4H), 8.02 (dd, J = 8.1, 1.4 Hz, 2H), 7.90 (ddd, J = 8.6, 7.0, 1.5 Hz, 2H), 7.74 – 7.68 (m, 2H), 7.55 (dd, J = 8.4, 7.2 Hz, 4H), 7.33 (d, J = 8.4 Hz, 2H), 5.21 (d, J = 17.8 Hz, 2H), 5.01 (d, J = 17.8 Hz, 2H), 4.02 – 3.95 (m, 2H), 3.30 – 3.23 (m, 2H). ^{13}C NMR (101 MHz, CD_3CN) δ 165.97, 147.91, 142.55, 137.49, 134.07, 132.81, 132.14, 130.68, 129.55, 129.42, 129.26, 121.37, 120.97, 69.51, 68.99, 32.33.

Re8. Yield 22%. MW 762.80 gmol^{-1}. Analytical RP-HPLC: t_R = 5.77 min. HR-MS (+, m/z, $[M]^+$): $[C_{30}H_{29}N_3O_3Re]^+$ calculated: 666.1761; found: 666.1750. ^{1}H NMR (400 MHz, CD_3CN) δ 8.47 (t, J = 8.4 Hz, 4H), 7.99 (dd, J = 8.1, 1.2 Hz, 2H), 7.87 (ddd, J = 8.7, 7.0, 1.5 Hz, 2H), 7.69 (t, J = 7.3 Hz, 2H), 7.53 (d, J = 8.5 Hz, 2H), 5.10 – 4.97 (m, 4H), 3.76 (d, J = 4.1 Hz, 2H), 2.07 – 2.02 (m, 2H), 1.80 (dt, J = 12.0, 2.8 Hz, 2H), 1.70 (dt, J = 12.8, 3.2 Hz, 1H), 1.42 (qt, J = 12.5, 3.2 Hz, 2H), 1.27 (tt, J = 12.4, 10.7 Hz, 4H). ^{13}C NMR (101 MHz, CD_3CN) δ 166.20, 147.79,

142.41, 133.96, 130.63, 129.43, 129.36, 129.18, 121.03, 75.62, 69.71, 36.57, 34.41, 26.91, 26.41.

Re9. Yield 21%. MW 750.79 gmol^{-1}. Analytical RP-HPLC: t_R = 5.75 min. ESI-MS (+, m/z, $[M]^+$): 654.29 $[C_{29}H_{29}N_3O_3Re]^+$. HR-MS (+, m/z, $[M]^+$): $[C_{29}H_{29}N_3O_3Re]^+$ calculated: 654.1761; found: 654.1751. ^{1}H NMR (400 MHz, CD3CN) δ 8.49 (t, J = 8.6 Hz, 4H), 8.01 (dd, J = 8.1, 1.2 Hz, 2H), 7.89 (ddd, J = 8.7, 7.1, 1.5 Hz, 2H), 7.70 (t, J = 7.6 Hz, 2H), 7.53 (d, J = 8.5 Hz, 2H), 5.07 (d, J = 17.9 Hz, 2H), 4.91 (d, J = 17.9 Hz, 2H), 3.82 – 3.73 (m, 2H), 1.97 (d, J = 8.1 Hz, 1H), 1.49 – 1.25 (m, 7H), 0.95 – 0.90 (m, 3H). ^{13}C NMR (101 MHz, CD3CN) δ 166.15, 147.87, 142.48, 134.01, 130.65, 129.48, 129.41, 129.19, 120.90, 69.58, 68.73, 32.20, 27.02, 26.68, 23.18, 14.25.

UV/vis spectroscopy

UV-vis spectra were recorded using a 1 cm quartz cuvette at room temperature. The stock solutions of the complexes were prepared at a concentration of 5 mM in DMSO and subsequently diluted to a final concentration of 50 µM in DMSO or 50 mM HEPES buffer (pH 7.4). To evaluate stability, the maximum absorption (320 nm) was monitored over an 18-hour incubation period using a plate reader (Tecan instrument Infinite M1000).

Antibacterial Activity

Unless otherwise stated sample preparation was performed in a class II biosafety cabinet. The samples were tested for their antimicrobial activity against *P. aeruginosa (PAO1), K. pneumoniae (Oxa-48), E. coli (W3110), A. baumannii (BAL225), Methicillin-resistant S. aureus (clinical isolate of MRSA), S. aureus Newman (patient isolate of MSSA), Bacillus subtilis (168 CA).* A colony of bacteria was grown in Luria-Bertani (LB) medium overnight at 37 °C. Stock solutions of 5 mM of the samples were prepared in DMSO and diluted to a starting concentration of 100 µM in Mueller Hinton (MH) medium. For the identification of the MIC the samples were two folds diluted. The bacterial concentration was determined by measuring the optical density at 600 nm and then diluted to an OD600 of 0.022 in MH medium. 5 µL of the diluted bacterial solution was used to inoculate 150 µL of the sample solutions, resulting in a final inoculation of about 5 × 10^5 CFU/mL. The plates were then incubated at 37 °C for 18 hours. For each assay, a control of broth only and a growth control of broth with bacterial inoculum without antibiotics were included in two columns of the plate. Polymyxin B and Vancomycin were used as control antibiotic for Gram-negative bacteria and Gram-positive bacteria respectively. The growth was measured by analysing the absorbance of the bacterial suspension at 600 nm using a plate reader (Tecan instrument Infinite M1000).

Haemolysis

Unless otherwise stated sample preparation was performed in a class II biosafety cabinet. The compounds were tested on human red blood cells (hRBCs) using a haemolysis assay as previously reported.[44] Blood was obtained from Interregionale Blutspende SRK AG in Bern, Switzerland. 1.5 mL of whole blood was centrifuged at 3000 rpm for 15 minutes at 4 °C, and the plasma was discarded. The hRBC pellet was washed three times with PBS (pH 7.4) and then resuspended to a final volume of 10 mL in PBS. For the determination of the MHC and HC_{50} of the compounds, the samples were two folds diluted starting from 200 µM, respectively. Samples stock solution was 20 mM in DMSO. Each plate included a blank medium control (PBS) and a haemolytic activity control (2% Triton TM X- 100). hRBC suspension was incubated with the samples in PBS in a V-shaped 96-well plate for 4 hours at 20 °C. After the

incubation, 100 µL of supernatant was carefully pipetted to a flat bottom, clear 96- wells plate. Haemolysis was measured by analysing the absorbance of free haemoglobin in the supernatants at 540 nm using a plate reader (Tecan instrument Infinite M1000). The percentage of haemolysis at each concentration was determined and the HC_{50} was calculated.

Cytotoxicity

The HEK293T human epithelial cells were purchased from the American Type Culture Collection (ATCC, Manassas, VA, USA). The cells were cultivated in DMEM high glucose supplemented (Merck) with 10% heat-inactivated fetal bovine serum, 100 UmL^{-1} of penicillin and streptomycin (Thermo Fisher Scientific) and maintained at a temperature of 37 °C with 5% CO_2. Initially, 4000 mL^{-1} of cells were seeded into 96-well plates and incubated for 18-24 hours before being exposed to compounds at concentrations ranging from 0.1 µM to 100 µM. Following a 24 hour incubation period at 37 °C, the cells were stained with alamar Blue HS Cell Viability Reagent (Thermo Fisher Scientific) and fluorescent was measured using a plate reader (Tecan instrument Infinite M1000). The control for the experiments was DMSO. Each sample was tested in at least three independent experiments. The concentration of a compound required to reduce cell growth by 50% compared to untreated control cells was determined as the half maximal cytotoxic concentration (CC_{50}).

Fluorescence Microscopy

Protocols were adapted from previous reported papers.[37] Fluorescence light microscopy was performed using a Nikon Ti-2 Eclipse,Nikon Europe BV, Amsterdam, Netherlands with a CFI Plan Fluor 40× oil immersion objective (CFI Plan Fluor 40×/1.30 W.D. 0.24, Nikon Europe BV). Brightfield and fluorescence images were recorded by an Andor Zyla 4.2 Plus USB3 camera in Widefield and using LED light excitation. Images were analyzed using ImageJ (Fiji). *Bacillus subtilis* PrpsD (MW54) expressing cytosolic GFP from the strong ribosomal PrpsD promoter was grown in LB at 37 °C under steady agitation in the presence of 100 µg/mL Spectinomycin. *Bacillus subtilis* MinD (KS69) was grown in LB at 37 °C under steady agitation in the presence of 50 µg/mL Spectinomycin. Overnight cultures of *B. subtilis* were regrown in LB (for MinD, 0.1% Xylose as an inducer is needed for the second culture). Rhenium complexes and controls were added at an OD_{600} of 0.3 and images were taken after 10 min of antibiotic treatment. Cells were immobilized on pre warmed 1.2% agarose-covered slides in HEPES buffer (50 mM pH 7.4)[45]. Membranes were stained with 1 µg/mL Nile red for 2 min. Nucleoids were stained with 1 µg/mL DAPI for 2 min.

Propidium iodide assay

Permeability for the large fluorescent molecule propidium iodide as a reporter for the presence of large membrane pores or severe membrane disruption was quantified using a Tecan Infinite M1000 plate reader, following the previously described protocol[41,46]. Bacteria were grown until an OD_{600} of 0.3 and antibiotics were added simultaneously with 13.3 µg/mL propidium iodide (1 mg/mL stock in DMSO). After 15 min, cells were centrifugated and the pallet washed twice with HEPES buffer (pH 7.4) and fluorescence was measured using 535 nm excitation and 617 nm emission wavelengths. SDS 0.05% served as positive control. Each experiment was performed in triplicate.

$DiOC_2$ assay

Membrane potential measurements were conducted using the potentiometric fluorescent probe 3,3'-dipropylthiadicarbocyanine iodide ($DiOC_2$) on a Tecan Infinite M1000 plate reader, following the previously described protocol[41,46]. Briefly, 1 µM $DiOC_2$ was added to exponentially growing *B. subtilis 168* cultures at 37 °C, and the baseline was recorded for 5 minutes using an excitation wavelength of 651 nm and an emission wavelength of 675 nm. **Re8** (3 µM), gramicidin (1 µg/mL, positive control) were then added, and samples were measured for an additional 20 minutes at 37 °C. Each experiment was performed in triplicate.

Sample preparation for SEM Imaging

Unless otherwise stated sample preparation was performed in a class II biosafety cabinet. A colony of *Bacillus subtilis (168 CA)* was grown in Luria-Bertani (LB) medium overnight at 37 °C. The bacteria concentration was measured by optical density at 600 nm until an OD_{600} of 0.3-0.4. 1 mL aliquots of the bacteria were prepared with subsequent addition of the compound and incubated at 37 °C for 10 min. Through centrifugation bacteria pellet were washed 3x with 50 mM HEPES (pH 7.4). Fixation, dehydrating, and drying methods were followed from the literature with minor modifications.[42,43] Cells pallet were chemically fixed using 2.5% (v/w) glutaraldehyde (Sigma-Aldrich) overnight in 50 mM HEPES, pH 7.4. The bacteria pellet underwent a graded dehydration series of ethanol (30, 50, 70, 80, 90, 100% for 10 min each) and HMDS (Fluka) drying (50 and 100% for 10 min each). The bacteria pellets were left dried overnight in a fume hood at room temperature. After drying, the samples were mounted on conductive carbon adhesive tape, sputter-coated with a layer of gold using Safematic CCU-010 sputter coater and viewed using a Gemini 450 scanning electron microscope at 5 kV.

Data Availability

We have provided all relevant data in the ESI of the paper.

Author contributions

A. F conceived the project. S. F. conducted all the syntheses, characterisations and biological assays. S.F., M. S., and A.F. analyzed the data. A. F. composed the manuscript. All authors discussed, commented and approved the final manuscript.

Conflicts of interest

There are no conflicts to declare.

Acknowledgements

We thank Prof. Jean-Louis Reymond for generously hosting and supporting our research group. Prof. Michaela Wenzel and Ann-Britt Schäfer are acknowledged for their introduction to BCP and providing the GFP-fused B. subtilis strains We also thank Prof. Christoph von Ballmoos and Nicola Dolder for access and introduction to their Fluorescence microscope. We thank Prof. Simon Grabowsky and Beatrice Frey for access to the SEM. We thank Çağrı Özsan for helpful comments and proofreading during the preparation of this manuscript. A. F. gratefully acknowledges funding from the Swiss National Science Foundation Ambizione grant PZ00P2_202016 and support by the University of Bern.

References

(1) Christensen, S. B. Drugs That Changed Society: History and Current Status of the Early Antibiotics: Salvarsan, Sulfonamides, and β-Lactams. *Molecules* **2021**, *26* (19), 6057. https://doi.org/10.3390/molecules26196057.
(2) Parascandola, J. From Mercury to Miracle Drugs: Syphilis Therapy over the Centuries. *Pharm. Hist.* **2009**, *51* (1), 14–23.
(3) Ligon, B. L. Penicillin: Its Discovery and Early Development. *Probl. Solut. Antimicrob. Resist. Pediatr. Respir. Tract Nosocomiall Pathog.* **2004**, *15* (1), 52–57. https://doi.org/10.1053/j.spid.2004.02.001.
(4) Hutchings, M. I.; Truman, A. W.; Wilkinson, B. Antibiotics: Past, Present and Future. *Curr. Opin. Microbiol.* **2019**, *51*, 72–80. https://doi.org/10.1016/j.mib.2019.10.008.
(5) Murray, C. J.; Ikuta, K. S.; Sharara, F.; Swetschinski, L.; Aguilar, G. R.; Gray, A.; Han, C.; Bisignano, C.; Rao, P.; Wool, E.; Johnson, S. C.; Browne, A. J.; Chipeta, M. G.; Fell, F.; Hackett, S.; Haines-Woodhouse, G.; Hamadani, B. H. K.; Kumaran, E. A. P.; McManigal, B.; Agarwal, R.; Akech, S.; Albertson, S.; Amuasi, J.; Andrews, J.; Aravkin, A.; Ashley, E.; Bailey, F.; Baker, S.; Basnyat, B.; Bekker, A.; Bender, R.; Bethou, A.; Bielicki, J.; Boonkasidecha, S.; Bukosia, J.; Carvalheiro, C.; Castañeda-Orjuela, C.; Chansamouth, V.; Chaurasia, S.; Chiurchiù, S.; Chowdhury, F.; Cook, A. J.; Cooper, B.; Cressey, T. R.; Criollo-Mora, E.; Cunningham, M.; Darboe, S.; Day, N. P. J.; Luca, M. D.; Dokova, K.; Dramowski, A.; Dunachie, S. J.; Eckmanns, T.; Eibach, D.; Emami, A.; Feasey, N.; Fisher-Pearson, N.; Forrest, K.; Garrett, D.; Gastmeier, P.; Giref, A. Z.; Greer, R. C.; Gupta, V.; Haller, S.; Haselbeck, A.; Hay, S. I.; Holm, M.; Hopkins, S.; Iregbu, K. C.; Jacobs, J.; Jarovsky, D.; Javanmardi, F.; Khorana, M.; Kissoon, N.; Kobeissi, E.; Kostyanev, T.; Krapp, F.; Krumkamp, R.; Kumar, A.; Kyu, H. H.; Lim, C.; Limmathurotsakul, D.; Loftus, M. J.; Lunn, M.; Ma, J.; Mturi, N.; Munera-Huertas, T.; Musicha, P.; Mussi-Pinhata, M. M.; Nakamura, T.; Nanavati, R.; Nangia, S.; Newton, P.; Ngoun, C.; Novotney, A.; Nwakanma, D.; Obiero, C. W.; Olivas-Martinez, A.; Olliaro, P.; Ooko, E.; Ortiz-Brizuela, E.; Peleg, A. Y.; Perrone, C.; Plakkal, N.; Ponce-de-Leon, A.; Raad, M.; Ramdin, T.; Riddell, A.; Roberts, T.; Robotham, J. V.; Roca, A.; Rudd, K. E.; Russell, N.; Schnall, J.; Scott, J. A. G.; Shivamallappa, M.; Sifuentes-Osornio, J.; Steenkeste, N.; Stewardson, A. J.; Stoeva, T.; Tasak, N.; Thaiprakong, A.; Thwaites, G.; Turner, C.; Turner, P.; Doorn, H. R. van; Velaphi, S.; Vongpradith, A.; Vu, H.; Walsh, T.; Waner, S.; Wangrangsimakul, T.; Wozniak, T.; Zheng, P.; Sartorius, B.; Lopez, A. D.; Stergachis, A.; Moore, C.; Dolecek, C.; Naghavi, M. Global Burden of Bacterial Antimicrobial Resistance in 2019: A Systematic Analysis. *The Lancet* **2022**, *399* (10325), 629–655. https://doi.org/10.1016/S0140-6736(21)02724-0.
(6) *Health and economic impacts of antimicrobial resistance in the Western Pacific Region, 2020–2030, 2023, WHO Regional Office for the Western Pacific*.
(7) *How to Overcome the Antibiotic Crisis: Facts, Challenges, Technologies and Future Perspectives*; Stadler, M., Dersch, P., Eds.; Current Topics in Microbiology and Immunology; Springer International Publishing: Cham, 2016; Vol. 398. https://doi.org/10.1007/978-3-319-49284-1.
(8) Gasser, G. Metal Complexes and Medicine: A Successful Combination. *CHIMIA* **2015**, *69* (7–8), 442. https://doi.org/10.2533/chimia.2015.442.
(9) Gamberi, T.; Chiappetta, G.; Fiaschi, T.; Modesti, A.; Sorbi, F.; Magherini, F. Upgrade of an Old Drug: Auranofin in Innovative Cancer Therapies to Overcome Drug Resistance and to Increase Drug Effectiveness. *Med. Res. Rev.* **2022**, *42* (3), 1111–1146. https://doi.org/10.1002/med.21872.
(10) Diaz, R. S.; Shytaj, I. L.; Giron, L. B.; Obermaier, B.; Della Libera, E.; Galinskas, J.; Dias, D.; Hunter, J.; Janini, M.; Gosuen, G.; Ferreira, P. A.; Sucupira, M. C.; Maricato, J.; Fackler, O.; Lusic, M.; Savarino, A.; SPARC Working Group. Potential Impact of the Antirheumatic Agent Auranofin on Proviral HIV-1 DNA in Individuals under Intensified Antiretroviral Therapy: Results from a Randomised Clinical Trial. *Int. J. Antimicrob. Agents* **2019**, *54* (5), 592–600. https://doi.org/10.1016/j.ijantimicag.2019.08.001.
(11) Capparelli Edmund V.; Bricker-Ford Robin; Rogers M. John; McKerrow James H.; Reed Sharon L. Phase I Clinical Trial Results of Auranofin, a Novel Antiparasitic Agent.

Antimicrob. Agents Chemother. **2016**, *61* (1), 10.1128/aac.01947-16. https://doi.org/10.1128/aac.01947-16.
(12) Harbut, M. B.; Vilchèze, C.; Luo, X.; Hensler, M. E.; Guo, H.; Yang, B.; Chatterjee, A. K.; Nizet, V.; Jacobs, W. R.; Schultz, P. G.; Wang, F. Auranofin Exerts Broad-Spectrum Bactericidal Activities by Targeting Thiol-Redox Homeostasis. *Proc. Natl. Acad. Sci.* **2015**, *112* (14), 4453–4458. https://doi.org/10.1073/pnas.1504022112.
(13) Brown, A.; Kumar, S.; Tchounwou, P. B. Cisplatin-Based Chemotherapy of Human Cancers. *J. Cancer Sci. Ther.* **2019**, *11* (4), 97.
(14) Galanski, M.; Jakupec, M. A.; Keppler, B. K. Update of the Preclinical Situation of Anticancer Platinum Complexes: Novel Design Strategies and Innovative Analytical Approaches. *Curr. Med. Chem. 12* (18), 2075–2094.
(15) Anthony, E. J.; Bolitho, E. M.; Bridgewater, H. E.; Carter, O. W. L.; Donnelly, J. M.; Imberti, C.; Lant, E. C.; Lermyte, F.; Needham, R. J.; Palau, M.; Sadler, P. J.; Shi, H.; Wang, F.-X.; Zhang, W.-Y.; Zhang, Z. Metallodrugs Are Unique: Opportunities and Challenges of Discovery and Development. *Chem. Sci.* **2020**, *11* (48), 12888–12917. https://doi.org/10.1039/D0SC04082G.
(16) Morrison, C. N.; Prosser, K. E.; Stokes, R. W.; Cordes, A.; Metzler-Nolte, N.; Cohen, S. M. Expanding Medicinal Chemistry into 3D Space: Metallofragments as 3D Scaffolds for Fragment-Based Drug Discovery. *Chem. Sci.* **2020**, *11* (5), 1216–1225. https://doi.org/10.1039/C9SC05586J.
(17) Lovering, F.; Bikker, J.; Humblet, C. Escape from Flatland: Increasing Saturation as an Approach to Improving Clinical Success. *J. Med. Chem.* **2009**, *52* (21), 6752–6756. https://doi.org/10.1021/jm901241e.
(18) Lovering, F. Escape from Flatland 2: Complexity and Promiscuity. *MedChemComm* **2013**, *4* (3), 515–519. https://doi.org/10.1039/C2MD20347B.
(19) Blaskovich, M. A. T.; Zuegg, J.; Elliott, A. G.; Cooper, M. A. Helping Chemists Discover New Antibiotics. *ACS Infect. Dis.* **2015**, *1* (7), 285–287. https://doi.org/10.1021/acsinfecdis.5b00044.
(20) Frei, A.; Zuegg, J.; Elliott, A. G.; Baker, M.; Braese, S.; Brown, C.; Chen, F.; G. Dowson, C.; Dujardin, G.; Jung, N.; King, A. P.; Mansour, A. M.; Massi, M.; Moat, J.; Mohamed, H. A.; Renfrew, A. K.; Rutledge, P. J.; Sadler, P. J.; Todd, M. H.; Willans, C. E.; Wilson, J. J.; Cooper, M. A.; Blaskovich, M. A. T. Metal Complexes as a Promising Source for New Antibiotics. *Chemical Science*, **2020**, *11*, 2627–2639. https://doi.org/10.1039/C9SC06460E.
(21) Frei, A.; Elliott, A. G.; Kan, A.; Dinh, H.; Bräse, S.; Bruce, A. E.; Bruce, M. R.; Chen, F.; Humaidy, D.; Jung, N.; King, A. P.; Lye, P. G.; Maliszewska, H. K.; Mansour, A. M.; Matiadis, D.; Muñoz, M. P.; Pai, T.-Y.; Pokhrel, S.; Sadler, P. J.; Sagnou, M.; Taylor, M.; Wilson, J. J.; Woods, D.; Zuegg, J.; Meyer, W.; Cain, A. K.; Cooper, M. A.; Blaskovich, M. A. T. Metal Complexes as Antifungals? From a Crowd-Sourced Compound Library to the First In Vivo Experiments. *JACS Au* **2022**, *2* (10), 2277–2294. https://doi.org/10.1021/jacsau.2c00308.
(22) Dilworth, J. R. Rhenium Chemistry – Then and Now. *Coord. Chem. Rev.* **2021**, *436*, 213822. https://doi.org/10.1016/j.ccr.2021.213822.
(23) Lo, K. K.-W. Luminescent Rhenium(I) and Iridium(III) Polypyridine Complexes as Biological Probes, Imaging Reagents, and Photocytotoxic Agents. *Acc. Chem. Res.* **2015**, *48* (12), 2985–2995. https://doi.org/10.1021/acs.accounts.5b00211.
(24) Hostachy, S.; Policar, C.; Delsuc, N. Re(I) Carbonyl Complexes: Multimodal Platforms for Inorganic Chemical Biology. *Coord. Chem. Rev.* **2017**, *351*, 172–188. https://doi.org/10.1016/j.ccr.2017.05.004.
(25) Schindler, K.; Zobi, F. Anticancer and Antibiotic Rhenium Tri- and Dicarbonyl Complexes: Current Research and Future Perspectives. *Molecules* **2022**, *27* (2), 539. https://doi.org/10.3390/molecules27020539.
(26) Bauer, E. B.; Haase, A. A.; Reich, R. M.; Crans, D. C.; Kühn, F. E. Organometallic and Coordination Rhenium Compounds and Their Potential in Cancer Therapy. *Coord. Chem. Rev.* **2019**, *393*, 79–117. https://doi.org/10.1016/j.ccr.2019.04.014.

(27) Wenzel, M.; Patra, M.; Senges, C. H. R.; Ott, I.; Stepanek, J. J.; Pinto, A.; Prochnow, P.; Vuong, C.; Langklotz, S.; Metzler-Nolte, N.; Bandow, J. E. Analysis of the Mechanism of Action of Potent Antibacterial Hetero-Tri-Organometallic Compounds: A Structurally New Class of Antibiotics. *ACS Chem. Biol.* **2013**, *8* (7), 1442–1450. https://doi.org/10.1021/cb4000844.
(28) Patra, M.; Wenzel, M.; Prochnow, P.; Pierroz, V.; Gasser, G.; Bandow, J. E.; Metzler-Nolte, N. An Organometallic Structure-Activity Relationship Study Reveals the Essential Role of a Re(CO)3 Moiety in the Activity against Gram-Positive Pathogens Including MRSA. *Chem. Sci.* **2014**, *6* (1), 214–224. https://doi.org/10.1039/C4SC02709D.
(29) Sovari, S. N.; Vojnovic, S.; Bogojevic, S. S.; Crochet, A.; Pavic, A.; Nikodinovic-Runic, J.; Zobi, F. Design, Synthesis and in Vivo Evaluation of 3-Arylcoumarin Derivatives of Rhenium(I) Tricarbonyl Complexes as Potent Antibacterial Agents against Methicillin-Resistant Staphylococcus Aureus (MRSA). *Eur. J. Med. Chem.* **2020**, *205*, 112533. https://doi.org/10.1016/j.ejmech.2020.112533.
(30) Sovari, S. N.; Radakovic, N.; Roch, P.; Crochet, A.; Pavic, A.; Zobi, F. Combatting AMR: A Molecular Approach to the Discovery of Potent and Non-Toxic Rhenium Complexes Active against C. Albicans-MRSA Co-Infection. *Eur. J. Med. Chem.* **2021**, *226*, 113858. https://doi.org/10.1016/j.ejmech.2021.113858.
(31) Mendes, S. S.; Marques, J.; Mesterházy, E.; Straetener, J.; Arts, M.; Pissarro, T.; Reginold, J.; Berscheid, A.; Bornikoel, J.; Kluj, R. M.; Mayer, C.; Oesterhelt, F.; Friães, S.; Royo, B.; Schneider, T.; Brötz-Oesterhelt, H.; Romão, C. C.; Saraiva, L. M. Synergetic Antimicrobial Activity and Mechanism of Clotrimazole-Linked CO-Releasing Molecules. *ACS Bio Med Chem Au* **2022**. https://doi.org/10.1021/acsbiomedchemau.2c00007.
(32) Frei, A.; Amado, M.; Cooper, M. A.; Blaskovich, M. A. T. Light-Activated Rhenium Complexes with Dual Mode of Action against Bacteria. *Chem. – Eur. J.* **2020**, *26* (13), 2852–2858. https://doi.org/10.1002/chem.201904689.
(33) Güntzel, P.; Nagel, C.; Weigelt, J.; Betts, J. W.; Pattrick, C. A.; Southam, H. M.; La Ragione, R. M.; Poole, R. K.; Schatzschneider, U. Biological Activity of Manganese(i) Tricarbonyl Complexes on Multidrug-Resistant Gram-Negative Bacteria: From Functional Studies to in Vivo Activity in Galleria Mellonella. *Metallomics* **2019**, *11* (12), 2033–2042. https://doi.org/10.1039/c9mt00224c.
(34) Betts, J. W.; Roth, P.; Pattrick, C. A.; Southam, H. M.; La Ragione, R. M.; Poole, R. K.; Schatzschneider, U. Antibacterial Activity of Mn(i) and Re(i) Tricarbonyl Complexes Conjugated to a Bile Acid Carrier Molecule. *Metallomics* **2020**, *12* (10), 1563–1575. https://doi.org/10.1039/d0mt00142b.
(35) Scaccaglia, M.; Birbaumer, M. P.; Pinelli, S.; Pelosi, G.; Frei, A. Discovery of Antibacterial Manganese(I) Tricarbonyl Complexes through Combinatorial Chemistry. *Chem. Sci.* **2024**. https://doi.org/10.1039/D3SC05326A.
(36) Schäfer, A.-B.; Wenzel, M. A How-To Guide for Mode of Action Analysis of Antimicrobial Peptides. *Front. Cell. Infect. Microbiol.* **2020**, *10*. https://doi.org/10.3389/fcimb.2020.540898.
(37) Wenzel, M.; Rautenbach, M.; Vosloo, J. A.; Siersma, T.; Aisenbrey, C. H. M.; Zaitseva, E.; Laubscher, W. E.; Van Rensburg, W.; Behrends, J. C.; Bechinger, B. The Multifaceted Antibacterial Mechanisms of the Pioneering Peptide Antibiotics Tyrocidine and Gramicidin S. *MBio* **2018**, *9* (5), e00802-18.
(38) Breukink, E.; Wiedemann, I.; Kraaij, C. van; Kuipers, O. P.; Sahl, H.-G.; de Kruijff, B. Use of the Cell Wall Precursor Lipid II by a Pore-Forming Peptide Antibiotic. *Science* **1999**, *286* (5448), 2361–2364. https://doi.org/10.1126/science.286.5448.2361.
(39) Wenzel, M.; Senges, C. H. R.; Zhang, J.; Suleman, S.; Nguyen, M.; Kumar, P.; Chiriac, A. I.; Stepanek, J. J.; Raatschen, N.; May, C.; Krämer, U.; Sahl, H.-G.; Straus, S. K.; Bandow, J. E. Antimicrobial Peptides from the Aurein Family Form Ion-Selective Pores in Bacillus Subtilis. *ChemBioChem* **2015**, *16* (7), 1101–1108. https://doi.org/10.1002/cbic.201500020.

(40) Wenzel, M.; Kohl, B.; Münch, D.; Raatschen, N.; Albada, H. B.; Hamoen, L.; Metzler-Nolte, N.; Sahl, H.-G.; Bandow, J. E. Proteomic Response of Bacillus Subtilis to Lantibiotics Reflects Differences in Interaction with the Cytoplasmic Membrane. *Antimicrob. Agents Chemother.* **2012**, *56* (11), 5749–5757. https://doi.org/10.1128/aac.01380-12.
(41) Müller, A.; Wenzel, M.; Strahl, H.; Grein, F.; Saaki, T. N. V; Kohl, B.; Siersma, T.; Bandow, J. E.; Sahl, H.-G.; Schneider, T.; Hamoen, L. W. Daptomycin Inhibits Cell Envelope Synthesis by Interfering with Fluid Membrane Microdomains. *Proc. Natl. Acad. Sci. USA* **2016**, *113*, E7077–E7086. https://doi.org/10.1073/pnas.1611173113.
(42) Golding, C. G.; Lamboo, L. L.; Beniac, D. R.; Booth, T. F. The Scanning Electron Microscope in Microbiology and Diagnosis of Infectious Disease. *Sci. Rep.* **2016**, *6* (1), 26516. https://doi.org/10.1038/srep26516.
(43) Shamprasad, B. R.; Lotha, R.; Nagarajan, S.; Sivasubramanian, A. Metal Nanoparticles Functionalized with Nutraceutical Kaempferitrin from Edible Crotalaria Juncea, Exert Potent Antimicrobial and Antibiofilm Effects against Methicillin-Resistant Staphylococcus Aureus. *Sci. Rep.* **2022**, *12* (1), 7061. https://doi.org/10.1038/s41598-022-11004-2.
(44) Zakharova, E.; Orsi, M.; Capecchi, A.; Reymond, J.-L. Machine Learning Guided Discovery of Non-Hemolytic Membrane Disruptive Anticancer Peptides. *ChemMedChem* **2022**, *17* (17), e202200291. https://doi.org/10.1002/cmdc.202200291.
(45) te Winkel, J. D.; Gray, D. A.; Seistrup, K. H.; Hamoen, L. W.; Strahl, H. Analysis of Antimicrobial-Triggered Membrane Depolarisation Using Voltage Sensitive Dyes. *Front. Cell Dev. Biol.* **2016**, *4*, 29. https://doi.org/10.3389/fcell.2016.00029.
(46) Saeloh, D.; Tipmanee, V.; Jim, K. K.; Dekker, M. P.; Bitter, W.; Voravuthikunchai, S. P.; Wenzel, M.; Hamoen, L. W. The Novel Antibiotic Rhodomyrtone Traps Membrane Proteins in Vesicles with Increased Fluidity. *PLoS Pathog.* **2018**, *14* (2), e1006876. https://doi.org/10.1371/journal.ppat.1006876.